Electrochemical DNA Biosensors for Detecting Nontuberculous Mycobacteria (NTM)

Dylan Poch[1,‡] & Tyler Sodia[1,‡], Jennifer R. Honda[2], Andrew J. Bonham[1,*].

[1]*Department of Chemistry & Biochemistry, Metropolitan State University of Denver, Denver, CO 80217-3362, USA. *e-mail: abonham@msudenver.edu*

[2]*Department of Biomedical Research and the Center for Genes, Environment, and Health, National Jewish Health, Denver, CO, USA*

[‡]*These authors contributed equally to this work.*

Abstract: Mycobacterial infection and mortality rates remain high; globally, an estimated 10 million cases of tuberculosis emerge each year caused by *Mycobacterium tuberculosis* (TB). However, the less studied species of nontuberculous mycobacteria (NTM) are becoming a growing concern. Over the last 30 years, NTM pulmonary disease cases have increased to outnumber TB in many regions. The "gold standard" for NTM diagnosis involves a weeks-to-month long microbiological culture-based method. We are developing a novel electrochemical biosensor to detect NTM that may ultimately be used as a more efficient diagnostic tool than the current, time-intensive methods. The molecular target of this biosensor is a complex lipoglycan, mannosylated lipoarabinomannan (ManLAM), abundantly found on the cell envelope of NTM and TB. The biosensor contains an electrode-bound DNA aptamer that changes conformational shape when bound to ManLAM. This conformational change is measured by voltammetric analysis, where a significant difference in electrochemical current upon binding of the ManLAM is observed. Future directions include optimizing this NTM biosensor to more robustly and sensitively detect ManLAM, as well as developing novel biosensors to target NTM-specific glycopeptidolipids (GPLs) to more directly target NTM. The ultimate expected outcome of this project is to improve rapid, point-of-care diagnostics that eliminate invasive sampling and lengthy culturing requirements and hence improve outcomes of patients with NTM infection.

Keywords: E-DNA; biosensor; nontuberculous mycobacteria (NTM); square wave voltammetry (SWV).

---

1. Introduction

The diverse genus of *Mycobacterium* consists of nearly 200 distinct species that are environmentally ubiquitous[1]. Many species of *Mycobacterium* are nonpathogenic organisms with others being obligate or opportunistic pathogens [1]. While, *Mycobacterium tuberculosis* (TB) is one of the world's pervasive causes of pulmonary infection and mortality[2,3], less known are the species of nontuberculous mycobacteria (NTM). Due partly to the "End TB Strategy" developed by the World Health Organization[4], TB infections have been reduced to approximately 3 cases per 100,000 individuals within the United States (U.S.) between 2013-2015[5]. However, NTM is a rapidly growing concern with the prevalence of NTM-related pulmonary disease growing at 8.2% annually (1997-2007)[6].

NTM, which are opportunistic lung pathogens found ubiquitously throughout the environment, are a growing public health concern. In the U.S. alone, there were nearly 100,000 NTM pulmonary infections and 2,990 deaths between 1999-2010 attributed to NTM[7,8]. Those with NTM pulmonary disease (NTM-PD) have an approximated 4.31-fold increased risk of respiratory failure and a five-year mortality rate > 25%[9,10]. Immunocompromised patients, such as individuals with HIV, are at heightened risk for disseminated infection and having the disease spread to other parts of the body such as the skin, joints, and

bones, among other organs; this often results in greatly increased mortality rates[11–13]. Furthermore, NTM is becoming an increasing financial burden; nearly $1.7 billion is spent annually in NTM-related expenses in the U.S[14].

While it depends on the species, common environmental niches to which NTM are well adapted include soils, lakes, and rivers, among other bodies of water[15]. Additionally, NTM are frequently found in water-distribution centers, swimming pools, showerheads, hospital ice machines, and heater coolers, along with many other man-made niches[15,16]. Inhalation of pathogenic aerosolized NTM is a common form of transmission which can result in NTM-PD[16]. Therefore, it is important to be able to efficiently research common sources of NTM and have the ability to rapidly identify NTM contaminated samples in such environments to mitigate the chance of transmission.

A rise in taxonomic classification and molecular methods has allowed for the identification of nearly 200 different NTM species, although only a handful of NTM species cause the majority of NTM-PD cases[1,17]. The *Mycobacterium avium* complex (MAC), which includes *M. avium* and *M. intracellulare,* is the most prevalent cause of NTM-related disease within the U.S.[18] MAC is also known to cause a majority of disseminated infections in immune-compromised individuals[19]. *M. abscessus* is another NTM species of concern, as it causes 65-80% of NTM-PD cases produced by rapid-growing NTM and shows increasing resistance to many established antibiotics. In some circumstances, NTM species have demonstrated a less efficacious response to commonly used antitubercular agents[20,21]. *M. kansasii* is a virulent NTM species and is within the top six most isolated NTM species from pulmonary samples globally[22–24]. Other etiologically important species include *M. chimaera*, *M. fortuitum*, *M. chelonae,* and *M. marinum*[25–27]

Despite the rising public health issues related to NTM infections, the current clinical diagnostic techniques used to detect such infections are non-ideal, primarily due to their lengthy time requirements. Currently, the "Gold Standard" for diagnosing NTM is culturing several microbiological samples from infected sputum or bronchoalveolar lavage before assigning an official diagnosis[28]. Depending on the NTM species, the time between collecting samples and making a diagnosis can take 6-8 weeks or longer[28].

With advances in diagnostic technology, recent strides have been made to reduce this diagnostic burden. This includes reducing the need for molecular expertise associated with the commonly utilized Polymerase Chain Reaction (PCR) and MALDI-TOF mass spectroscopy methods, among lesser-used techniques of NTM identification such as Raman Spectroscopy and luciferase reporter mycobacteriophages for MGIT cultures [29–32]. However, all of these techniques require sophisticated instrumentation and molecular expertise that may not be readily available in a clinical laboratory.

To alleviate this diagnostic dilemma and shorten the window of time to successful patient intervention, we propose a biosensor-based strategy for NTM detection. Biosensors are devices that detect molecular targets using a biological-based sensing mechanism[33–35]. Specifically, a molecular target from a sample (*e.g*., components of a bacterial cell wall or other identifying markers) will be bound by a biological component in the biosensor (*e.g.,* DNA, RNA, antibodies, enzymes, etc.). This binding event triggers a change in the biosensor that leads to a measurable readout indicating the presence or absence of the molecular target in the sample tested. Biosensors have rapidly integrated into a wide variety of fields including forensics, food industry, agriculture, and most notably, medical diagnostics[34,36–39]. While there are many diverse architectural designs of biosensing devices, some of the more common designs include electrochemical, optical, magnetic, and immune/enzymatic-based sensors [40,41]. Biosensors have already been applied toward the detection of bacteria in biological specimens including sputum, feces, and whole-cell detection[41–43].

Electrochemical DNA-based biosensors (E-DNA biosensors) have previously shown reliable detection at extremely low concentrations (picomolar concentrations)[34] of target proteins and drugs. E-DNA biosensors have been used in the detection of antibodies, cancer biomarkers, chemotherapeutics such as doxorubicin, as well as IP-10 (an immune rejection marker for surgical tissue transplants), among many other targets [35,44–48]. Our lab previously developed E-DNA biosensors capable of rapidly and reliably detecting the presence of both ricin and botulinum toxins in serum[49]. Since E-DNA biosensors are sensitive, robust, and rapid devices capable of detecting a myriad of complex biological molecules, they hold great promise in efficient point-of-care (POC) clinical

diagnostics. This would significantly reduce the time between the onset of symptoms and appropriate treatment regimes. However, these E-DNA biosensors have not been applied to detect the presence of NTM-specific targets in clinical or environmental samples.

In this study, we have designed an E-DNA biosensor for the detection of NTM. E-DNA biosensors often employ a single-stranded DNA (ss-DNA) sequence to selectively recognize and bind to a specific analyte[50,51]. The ss-DNA, employed as an aptamer, is linked to a redox indicator moiety such as methylene blue (MB) or ferrocene[51]. The aptamer probe is first immobilized onto a gold electrode to serve as a transducer which will convert physical changes (*e.g.,* bonding, shape, or flexibility) of the probe into a redox current that can be quantified and analyzed[51,52]. This physical change is caused by a DNA binding event (the analyte binds to the ssDNA probe), resulting in a change in proximity or availability of the redox label to the electrode[52]. This change in output is proportional to the concentration of the analyte and can thus be analyzed to determine the concentration of the analyte in a sample.

A mycobacterial-specific glycolipid, mannosylated lipoarabinomannan (ManLAM), was used as the initial molecular target for detecting NTM. Found on the cell wall of many pathogenic species of NTM (**Fig. 1, a**)**,** ManLAM consists of an arabinan polymer with both branched and linear arabinofuranosides that include distal mannosylated caps, as well as fatty acyl tails anchoring the structure onto the cell membrane (**Fig. 1, b**) [7,53]. ManLAM was chosen due to both the pre-existing availability of an aptamer sequence that binds to ManLAM as well as the prevalence of this target, specifically the lipoarabinomannan backbone, in most pathogenic mycobacteria [7,54,55]. This POC approach may improve patient outcomes and reduce the morbidity and mortality rates by providing an alternative to the lengthy diagnostics that currently surround NTM infection.

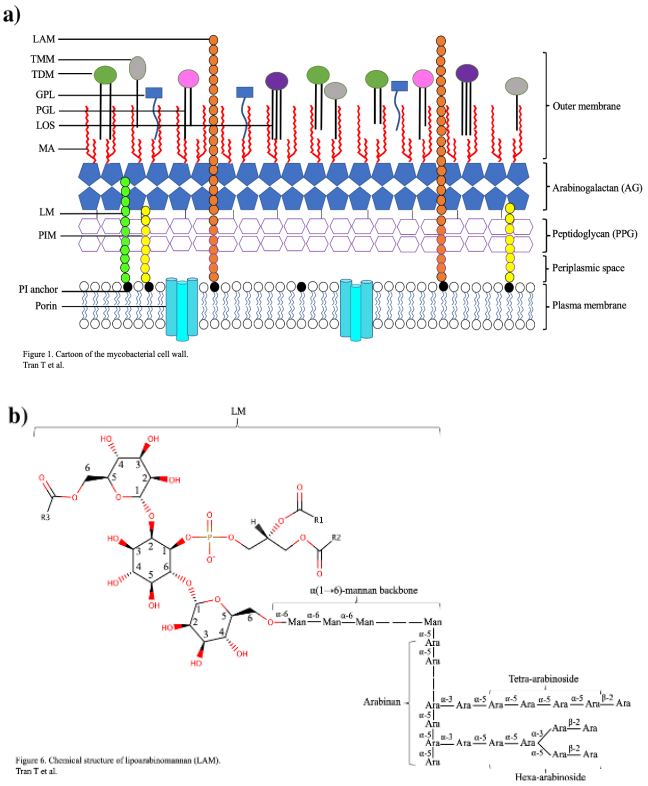

Fig.1. (a) Typical extracellular matrix of a mycobacterial cell wall. Of note, LAM molecules are shown as orange circles, and GPL is shown as blue rectangles. (b) Molecular structure of LAM. Used with permission[7].

2. Methods

2.1. Aptamer Sequence & Biosensor Design

The original ManLAM-specific aptamer sequence (**Fig. 2**) was previously identified using systematic evolution of ligands by exponential enrichment (SELEX) methodology [55]. This aptamer sequence, called BM2, had the following nucleotide sequence:

5’- GCG GAA TTC TAA TAC GAC TCA CTA TAG GGA ACA GTC CGA GCC CCC CAT GAA CTA GGC TCC ACA ATG AGT TTG GGG GTC AAT GCG TCA TAG GAT CCC GC -3’

The N31 region (denoting the region randomized during the SELEX procedure) of the BM2 aptamer (**Fig. 2**, red box) was reported to have a high affinity for ManLAM, due to its low dissociation constant (K_D) (see Results 3.2). To evaluate multiple sequence variants of the N31 region within the BM2 aptamer, a predictive software program, *Quikfold,* was utilized for the structure of single-stranded nucleic acids [56]. Using *Quickfold*, the N31 region was altered to allow the aptamer to support two isoenergetic conformational states in response to ManLAM binding **(Fig. 3).**

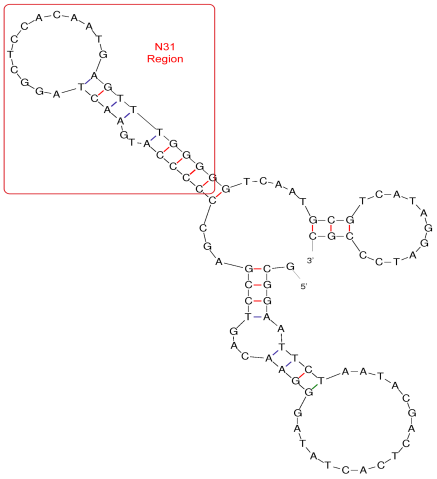

Fig.2. Schematic of the original BM2 aptamer sequence previously identified[55]. The N31 region (red outline) was where selective binding to ManLAM was predicted to have the greatest affinity.

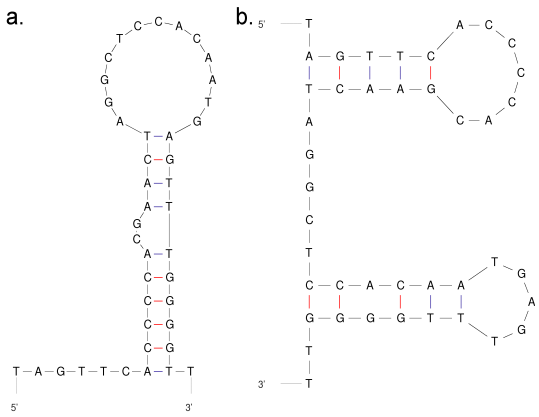

Fig.3. First version of biosensor based on minimally modified N31 region of BM2 aptamer. **a.** functional "On" conformational state when the aptamer binds to the ManLAM target. **b.** alternative "Off" conformation when unbound.

Our initial design was synthesized via standard oligonucleotide synthesis (Biosearch Technologies, Hoddesdon, UK). However, initial experiments with this construct using square-wave voltammetry (SWV) interrogation indicated that this initial biosensor version was inadequate at generating a signal indicative of a binding interaction. To address this, we investigated a series of partial truncations of the original BM2 aptamer sequences. A final version of our aptamer biosensor (**Fig. 4**) has the following nucleotide sequence:

5'- CTC ACT ATA GGG AAC AGT CCG AGC CCC CCA TGA ACT AGG CTC CAC AAT GAG TTT GGG GGT TTC T(Methylene Blue)CA TCT GGT TTG ACT G -3'

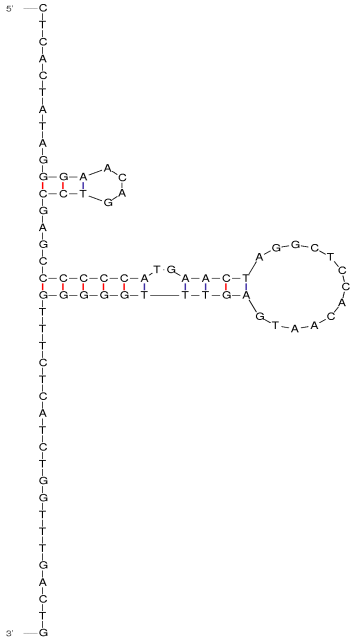

Fig.4. Final truncated BM2 aptamer sequence that yielded an observed K_D of 15 ± 10 nM in fluorescence anisotropy evaluation. Image depicts predicted binding state.

After determining the appropriate aptamer sequence, an E-DNA biosensor was generated to detect ManLAM. The aptamer probe was synthesized with the following two modifications to effectively function as an electrochemical biosensing element. First, a redox moiety of MB was covalently linked to a thymine base at position T64. Second, a 5' thiol was introduced to facilitate attachment of the oligonucleotide to a gold electrode via thiol-gold coupling.

2.2. Anisotropic Analysis

Fluorescence anisotropy was used to determine the binding affinity of the final ManLAM truncated aptamer sequence (**Fig. 4**). The parameters utilized for anisotropy trials were: excitation wavelength = 480 nm - 500 nm, with a 1 nm slit; emission wavelength = 520 nm, with a 1 nm slit; integration time was set to 1 second. A 50 µL, 10 mm sub-micro quartz fluorometer cell (Starna Cells, Atascadero, CA) was filled with 200 µL binding buffer (49.45 mM NaCl, 20 mM TRIS (tris (hydroxymethyl) amino-methane), 66.7 mM CaCl2, and 12.6 mM MgCl2 in 900 mL of nanopore H_2O, pH-adjusted to 7.10) along with 1 µL of our DNA aptamer. Target ManLAM was sequentially added in five-minute increments. The ManLAM (1 mg/mL) was harvested from TB H37Rv.

2.3. Electrode Preparation and Biosensor Attachment

Ceramic screen-printed gold electrodes (Pine Research Instrumentation, Durham, North Carolina) with a 1 mm^2 working electrode surface area and an Ag/AgCl pseudo-reference electrode were used. Before electrochemically testing the biosensor, the electrodes were thoroughly cleaned with the following protocol: a solution of 0.5 M NaOH was added dropwise to the electrode followed by cyclic voltammetry (CV) cleaning. (initial potential= -0.4 V, final potential= -0.4 V, upper potential= -0.4 V, lower potential = -1.35 V, segments = 100, sweep rates = 2 V/s.)

Next, the NaOH was removed and 0.5 M H_2SO_4 was added before CV cleaning was conducted (first run: period= 0 mV—3 s, electrolysis period = 2 V—3 S, relaxation period= 0 mV—1 S; second run: induction period= 0 mV—3 s, electrolysis period = -0.35 V—10 s, relaxation period= 0 mV—1 s; third run: initial potential= -0.35 V, final potential= -0.35 V, upper potential= 1.5 V, lower potential= -0.35 V, segments= 20, sweep rates= 4 V/s; fourth run: initial potential= -0.35 V, final potential= -0.35 V, upper potential= 1.5 V, lower potential= 0.35 V, segments= 4, sweep rates= 0.1 V/s.)

The H_2SO_4 was replaced with 0.1 M H_2SO_4/0.01 M KCl and cycled using (first run: initial potential= 0.2 V, final potential= 0.2 V, upper potential= 0.75 V, lower potential= 0.2 V, segments= 10, sweep rates= 0.1 V/s; second run: initial potential= 0.2 V, final potential= 0.2 V, upper potential= 1 V, lower potential= 0.2 V, segments= 10, sweep rates= 0.1 V/s; third run: initial potential= 0.2 V, final potential= 0.2 V, upper potential= 1.25 V, lower potential= 0.2 V, segments=10, sweep rates= 0.1 V/s; fourth run: initial potential= 0.2 V, final potential= 0.2 V, upper potential= 1.5 V, lower potential= 0.2 V, segments= 10, sweep rates= 0.1 V/s.)

Finally, the 0.1 M H_2SO_4/0.01 M KCl solution was replaced with 0.05 M H_2SO_4 and a final CV cleaning was conducted (initial potential= -0.35 V, final potential= -0.35 V, upper potential= 1.5 V, lower potential= -0.35 V, segments= 4, sweep rates= 0.1 V/s.)

A sample of 1 µL tris(2-carboxyethyl) phosphine hydrochloride (TCEP) and 3 µL DNA biosensor was allowed to equilibrate on ice for > 20 minutes to activate the thiol for attachment. The 0.05 M H_2SO_4 was removed from the electrode. Then 96 µL of the binding buffer was added to the TCEP/DNA solution and applied to the electrode to equilibrate for > 45 minutes. Next, the DNA-containing solution was removed, and the electrode was covered with 300 µL of 2 mM 1-mercapto-6-hexanol to chemically passivate the surface to avoid biosensor fouling for > 35 minutes. Finally, the electrode was submerged in binding buffer and 200 µL of the same binding buffer was added to the electrode surface.

2.4. Electrochemical Parameters and Analytical Methods

After the electrode was cleaned and the biosensor was attached, sensor behavior was analyzed using a WaveNano potentiostat and its software control program, *Aftermath* (both from Pine Research Instrumentation). The potentiostat allowed the change in current to be measured using the voltammetric electrochemical technique of SWV. This technique is similar to cyclic voltammetry (CV) but has an increased limit of detection (LOD), faster measurement rates, and additional parameters to optimize signal response[57].

For SWV trials the following parameters were used: initial potential of -0.5 V, final potential of 0 V, amplitude of 50 mV, period 0.004 s (subject to change, see Results 3.3), increment of 0.5 mV, sampling width of 0.001 s, duration of 1 s, initial range of 50 µA, and induction potential of -400 mV. The blank sensor response was measured at 0 minutes, 15 minutes, and 30 minutes. Serial dilutions of purified

ManLAM were then added to the electrode. Purified ManLAM was obtained from Dr. Jennifer R. Honda in the Department of Biomedical Research and the Center for Genes, Environment, and Health, National Jewish Health, Denver, CO, USA. Solutions were equilibrated for five minutes before SWV interrogation and addition of the next concentration. Differences in SWV peak height were analyzed using custom peak fitting software SWV *AnyPeakFinder:* https://github.com/Paradoxdruid/SWVAnyPeak-Finder)[58]. For more detailed information on electrochemical E-DNA biosensor preparation, cleaning, and parameters, see previous work by Rowe et al[59].

3. Results & Discussion

3.1. Truncated Aptamer Biosensor

The final truncated N31 aptamer sequence (**Fig. 4**) was designed to allow for two isoenergetic conformational states. These isoenergetic conformations allow the nucleotide probe to share a ManLAM binding-capable (On) and a non-binding alternative (Off) state. The functional (binding) state has a high affinity to bind ManLAM. This binding causes changes in the folding dynamics which allows the methylene blue moiety to more efficiently interact with the gold electrode due to closer proximity (**Fig. 5**)**.**

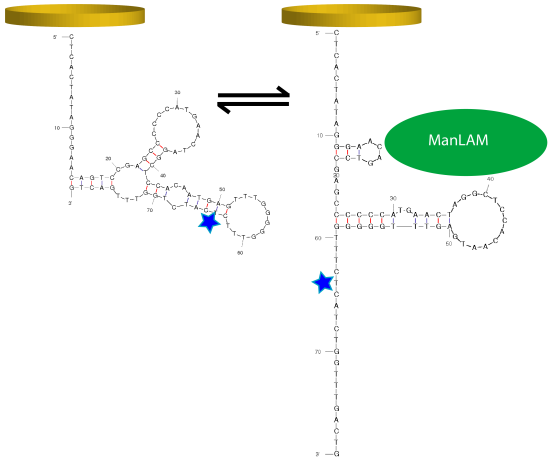

Fig.5. Schematic of the final version biosensor with 5'-thiol linkage to the gold electrode and methylene blue moiety (blue star) attached to internal thymidine. (left) non-binding state and (right) binding-capable state with green ManLAM predicted binding site.

The increased interaction efficiency results in a greater redox current. However, the alternative non-binding state is unable to bind to the target, resulting in a diminished electrical current. When ManLAM is present, the binding-capable conformational state will predominate, generating a measurable change in redox output. Therefore, the redox current generated by the conformational change of the aptamer is directly related to the concentration of the molecular target. At 25 °C, these two conformational states were designed to be isoenergetic (having the same folding energy) with the predicted ratio of both states being 1:1 to allow a balance of the detection limit and measurability of change in electrical current upon binding[60].

3.2. Aptamer Anisotropy

Fluorescence anisotropy precisely measures the change in fluorescent emission when a vertically polarized ray of light strikes the fluorophore[61,62], producing horizontal and vertical polarized emissions that share a ratio. This ratio will be dependent upon the rotational rate of the molecular target being analyzed[61]. When the aptamer binds to ManLAM, the rotation speed decreases due to the increase in mass, which leads to changes in the anisotropy value.

The results from the six anisotropy experiments (Methods 2.2**)** were used to construct a binding curve (**Fig. 6**)**.** That binding was calculated using a standard Langmuir isotherm, allowing determination of an apparent K_D of 15 ± 10 nM. Other methods (electrophoretic mobility shift assays (EMSA), UV/Vis spectroscopy, and thermo cyclic melt curve analysis) were used to verify binding; however, results were inconsistent and considered insignificant. We believe that these inconsistencies stem both from the lipidated nature of ManLAM and unwanted indicator fluorophore binding to ManLAM**.**

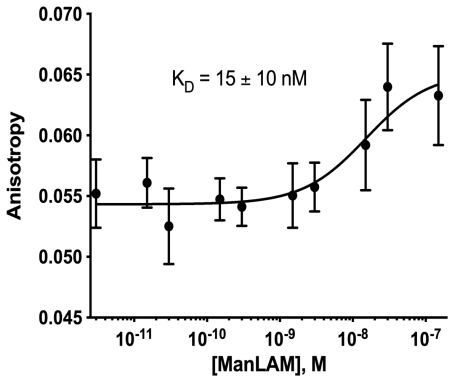

Fig.6. ManLAM was titrated from concentrations between 10^{-11} to 10^{-7}M. Nonlinear regression to a Langmuir isotherm binding model shows a direct correlation between increase in ManLAM concentration with increased anisotropy values. Apparent K_D of 15 ± 10 nM.

3.3. Electrochemical Analysis

At present, we are still actively gathering SWV data and, therefore, are unable to draw any definitive conclusions relating to our biosensor's electrochemical performance. Currently, the data obtained from preliminary trials infer a direct change in electrochemical current with increased concentrations of added ManLAM (**Fig. 7**). This is due to the functional conformational state moving the redox moiety (methylene blue) closer to the electrode. We expect that this will allow us to extrapolate the concentration of ManLAM relative to the solution.

While the aptamer has strong evidence of binding (**Fig. 6**) and a preliminary direct change in current when exposed to increased relative concentrations of ManLAM (**Fig. 7**), the changes in current have been inconclusive in regards to generating a consistent increased (signal-On) versus decreased (signal-Off) current. These issues are currently being addressed through varying the frequency of interrogation, which has previously been an identified factor when it comes to E-DNA biosensors switching between gain-of-signal vs loss-of-signal[63]. Furthermore, the concentration of DNA aptamer density on the gold surface electrode has been shown to be a factor in optimizing consistent signal responses in E-DNA biosensors (*i.e.,* having a signal-On vs signal-Off response)[64]. Therefore, the concentration of the DNA aptamer will be adjusted to improve the efficacy and reproducibility of the biosensor. Finally, the predictive software program Quickfold[56] indicates that temperature may play an integral role in the binding affinity of our target by changing the molecular structure of the aptamer at varying temperatures. Further research is needed to determine if a change in temperature may result in alteration of binding affinity for this target.

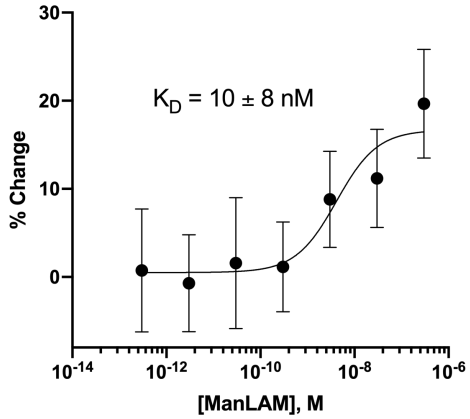

Fig.7. Normalized signal data obtained from several SWV trials resulted in a direct gain-of-signal. However, the biosensor has also demonstrated direct change with the occasional loss-of-signal during other SWV trials. This issue of reproducibility is currently under investigation.

3.4. Future Directions

In addition to the aforementioned efforts to obtain more consistent biosensor evidence, the next step includes expanding the scope of the project to include other targets for NTM detection. One potential target is the glycopeptidolipid (GPL). As ManLAM is found on both TB and NTM, it is not specific enough to be classified as a biosensor specific to NTM. GPLs, in contrast, are found within the cell walls of many of the major NTM species of interest (including *M. avium, M. intracellulare, M. abscessus,* and *M. chelonae*), while being absent from TB[7,65]. However, to detect GPL, a new aptamer sequence would need to be generated. We plan to undertake this process using SELEX[66]. Overall, creating a GPL-specific E-DNA biosensor would increase sensor specificity.

After discovering and validating binding with a suitable aptamer for GPL, the new aptamer sequence

will be subjected to voltammetric interrogation as previously discussed in Methods 2.3 & 2.4. The electrochemical redox current output will be measured allowing the extrapolation of the concentration of GPL relative to the solution. The anticipated outcome is to create a biosensor capable of rapid GPL identification for the detection of NTM in both medical and environmental samples.

Finally, in our ambition to develop a medically relevant biosensor, we intend to expand the scope of this project by starting trials involving patient samples. This will be accomplished by SWV interrogation using total lipid extracts from respiratory isolates of NTM including *M. avium*, *M. intracellulare*, *M. chimaera*, *M. abscessus*, and TB (H37Rv) total lipid extracts (BEI Resources, Manassas, VA: NR-14837). We are currently working to improve the robustness and sensitivity of the sensor to allow detection of ManLAM in complex media including these lipid extracts. Additionally, we plan to investigate the change in the biosensor's specificity and intensity in response to isolated LAM variants of different species of *Mycobacteria* such as *M. leprae* and *M. smegmatis*. Ultimately, we aim to test the robustness of our biosensor in other forms of complex media, such as blood or sputum.

Overall, this project illustrates a work-in-progress on the creation of a sensitive E-DNA biosensor that can detect the presence of NTM using the molecular target, ManLAM. Although the project is currently incomplete (that is, the signal patterns are inconsistent and only tested in buffer solutions), we are continuously adopting strategies to resolve these inconsistencies and are expanding the scope of the project to reduce such restrictions. The use of such a biosensor could have great benefits to medical and environmental sensing. Such a biosensor would be able to drastically reduce the time required for NTM identification and assessment and bolster appropriate treatment interventions. In turn, this could greatly increase patient outcomes by reducing morbidity and mortality rates that are currently associated with NTM infections worldwide.

Acknowledgments:

The authors thank Grant Norton, National Jewish Health, for helpful discussion and preparation of LAM samples. The authors also thank Dr. Megan Filbin, MSU Denver, for helpful discussion and troubleshooting. The authors thank the MSU Denver Undergraduate Research Program for grants and other support.

4. References

(1) Matsumoto, Y.; Kinjo, T.; Motooka, D.; Nabeya, D.; Jung, N.; Uechi, K.; Horii, T.; Iida, T.; Fujita, J.; Nakamura, S. Comprehensive Subspecies Identification of 175 Nontuberculous Mycobacteria Species Based on 7547 Genomic Profiles. *Emerg. Microbes Infect.* **2019**, *8* (1), 1043–1053. https://doi.org/10.1080/22221751.2019.1637702.

(2) Houben, R. M. G. J.; Dodd, P. J. The Global Burden of Latent Tuberculosis Infection: A Re-Estimation Using Mathematical Modelling. *PLOS Med.* **2016**, *13* (10).

(3) World Health Organisation. Global Tuberculosis Report 2015. Geneva. **2015**.

(4) Lobue, P. A.; Mermin, J. H. Latent Tuberculosis Infection: The Final Frontier of Tuberculosis Elimination in the USA. *Lancet Infect. Dis.* **2017**, *17* (10).

(5) Salinas, J. L.; Mindra, G.; Haddad, M. B.; Pratt, R.; Price, S. F.; Langer, A. J. Leveling of Tuberculosis Incidence — United States, 2013–2015. *MMWR. Morb. Mortal. Wkly. Rep.* **2016**, *65* (11), 273–278.

(6) Adjemian, J.; Olivier, K. N.; Seitz, A. E.; Holland, S. M.; Prevots, D. R. Prevalence of Nontuberculous Mycobacterial Lung Disease in U.S. Medicare Beneficiaries. *Am. J. Respir. Crit. Care Med.* **2012**. https://doi.org/10.1164/rccm.201111-2016OC.

(7) Tran, T.; Bonham, A. J.; Chan, E. D.; Honda, J. R. A Paucity of Knowledge Regarding Nontuberculous Mycobacterial Lipids Compared to the Tubercle Bacillus. *Tuberculosis* **2019**, *115*, 96–107. https://doi.org/10.1016/J.TUBE.2019.02.008.

(8) Mirsaeidi, M.; Machado, R. F.; Garcia, J. G. N.; Schraufnagel, D. E. Nontuberculous Mycobacterial Disease Mortality in the United States, 1999–2010: A Population-Based Comparative Study. *PLoS One* **2014**, *9* (3), e91879. https://doi.org/10.1371/journal.pone.0091879.

(9) Yeh, J. J.; Wang, Y. C.; Lin, C. L.; Chou, C. Y. T.; Yeh, T. C.; Wu, B. T.; Sung, F. C.; Kao, C. H. Nontuberculous Mycobacterial Infection Is Associated with Increased Respiratory Failure: A Nationwide Cohort Study. *PLoS One* **2014**, *9* (6). https://doi.org/10.1371/journal.pone.0099260.

(10) Diel, R.; Lipman, M.; Hoefsloot, W. High Mortality in Patients with Mycobacterium Avium Complex Lung Disease: A Systematic Review. *BMC Infect. Dis.* **2018**, *18* (1).

(11) Tortoli, E. Clinical Manifestations of Nontuberculous Mycobacteria Infections. *Clin. Microbiol. Infect.* **2009**, *15* (10), 906–910.

(12) Kobayashi, T.; Nishijima, T.; Teruya, K.; Aoki, T.; Kikuchi, Y.; Oka, S.; Gatanaga, H. High Mortality of Disseminated Non-Tuberculous Mycobacterial Infection in HIV-Infected Patients in the Antiretroviral Therapy Era. *PLoS One* **2016**, *11* (3).

(13) Ristola, M. A.; Reyn, C. V.; Arbeit, R. D.; Soini, H.; Lumio, J.; Ranki, A.; Bühler, S.; Waddell, R.; Tosteson, A. N.; Falkinham, J.; Sox, C. H. High Rates of Disseminated Infection Due to Non-Tuberculous Mycobacteria among AIDS Patients in Finland. *J. Infect.* **1999**, *39* (1), 61–67.

(14) Strollo, S. E.; Adjemian, J.; Adjemian, M. K.; Prevots, D. R. The Burden of Pulmonary Nontuberculous Mycobacterial Disease in the United States. *Ann. Am. Thorac. Soc.* **2015**, *12* (10), 1458–1464. https://doi.org/10.1513/AnnalsATS.201503-173OC.

(15) Honda, J. R.; Virdi, R.; Chan, E. D. Global Environmental Nontuberculous Mycobacteria and Their Contemporaneous Man-Made and Natural Niches. *Front. Microbiol.* **2018**, *9*. https://doi.org/10.3389/fmicb.2018.02029.

(16) Halstrom, S.; Price, P.; Thomson, R. Review: Environmental Mycobacteria as a Cause of Human Infection. *Int. J. Mycobacteriology* **2015**, *4* (2), 81–91. https://doi.org/10.1016/j.ijmyco.2015.03.002.

(17) Johnson, M. M.; Odell, J. A. Nontuberculous Mycobacterial Pulmonary Infections. *J. Thorac. Dis.* **2014**, *6* (3), 210–220. https://doi.org/10.3978/j.issn.2072-1439.2013.12.24.

(18) Griffith, D. E.; Aksamit, T.; Brown-Elliott, B. A.; Catanzaro, A.; Daley, C.; Gordin, F.; Holland, S. M.; Horsburgh, R.; Huitt, G.; Iademarco, M. F.; et al. An Official ATS/IDSA Statement: Diagnosis, Treatment, and Prevention of Nontuberculous Mycobacterial Diseases. *Am. J. Respir. Crit. Care Med.* **2007**, *175* (4), 367–416. https://doi.org/10.1164/rccm.200604-571ST.

(19) Guglielmetti, L.; Mougari, F.; Lopes, A.; Raskine, L.; Cambau, E. Human Infections Due to Nontuberculous Mycobacteria: The Infectious Diseases and Clinical Microbiology Specialists' Point of View. *Future Microbiol.* **2015**, *10* (9), 1467–1483.

(20) Koh, W.-J.; Jeon, K.; Lee, N. Y.; Kim, B.-J.; Kook, Y.-H.; Lee, S.-H.; Park, Y. K.; Kim, C. K.; Huitt, G. A.; Daley, C. L.; Kwon, O. J. Clinical Significance of Differentiation of Mycobacterium Massiliense from Mycobacterium Abscessus. *Am. J. Resp. Crit. Care Med.* **2010**, *183* (3).

(21) Diagnosis and Treatment of Disease Caused by Nontuberculous Mycobacteria. *Am. J. Respir. Crit. Care Med.* **1997**, *156* (2).

(22) Moon, S. M.; Park, H. Y.; Jeon, K.; Kim, S.-Y.; Chung, M. J.; Huh, H. J.; Ki, C.-S.; Lee, N. Y.; Shin, S. J.; Koh, W.-J. Clinical Significance of Mycobacterium Kansasii Isolates from Respiratory Specimens. *PLoS One* **2015**, *10* (10).

(23) Kwon, Y.-S.; Koh, W.-J. Diagnosis and Treatment of Nontuberculous Mycobacterial Lung Disease. *J. Korean Med. Sci.* **2016**, *31* (5).

(24) Liu, C.-J.; Huang, H.-L.; Cheng, M.-H.; Lu, P.-L.; Shu, C.-C.; Wang, J.-Y.; Chong, I.-W. Outcome of Patients with and Poor Prognostic Factors for Mycobacterium Kansasii-Pulmonary Disease. *Respir. Med.* **2019**, *151*, 19–26.

(25) Hasan, N. A.; Honda, J. R.; Davidson, R. M.; Epperson, L. E.; Bankowski, M. J.; Chan, E. D.; Strong, M. Complete Genome Sequence of Mycobacterium Chimaera Strain AH16. *Genome Announc.* **2016**, *4* (6).

(26) The Many Lives of Nontuberculous Mycobacteria. Claeys, T. A.; Robinson, R. T. *J. Bacteriol.* **2018**, *200* (11).

(27) Pinto-Gouveia, M.; Gameiro, A.; Ramos, L.; Cardoso, J. C.; Brites, M. M.; Tellechea, S.; Figueiredo, A. R. Mycobacterium Chelonae Is an Ubiquitous Atypical Mycobacterium. *Case Rep. Dermatol.* **2015**, *7* (2), 207–211.

(28) Forbes, B. A.; Hall, G. S.; Miller, M. B.; Novak, S. M.; Rowlinson, M.-C.; Salfinger, M.; Somoskövi, A.; Warshauer, D. M.; Wilson, M. L. Practice Guidelines for Clinical Microbiology Laboratories: Mycobacteria. *Clin. Microbiol. Rev.* **2018**, *31* (2).

(29) Scoleri, G. P.; Choo, J. M.; Leong, L. E. X.; Goddard, T. R.; Shephard, L.; Burr, L. D.; Bastian, I.; Thomson, R. M.; Rogers, G. B. Culture-Independent Detection of Nontuberculous Mycobacteria in Clinical Respiratory

Samples. *J. Clin. Microbiol.* **2016**, *54* (9), 2395–2398. https://doi.org/10.1128/JCM.01410-16.

(30) Erkose Genc, G.; Demir, M.; Yaman, G.; Kayar, B.; Koksal, F.; Satana, D. Evaluation of MALDI-TOF MS for Identification of Nontuberculous Mycobacteria Isolated from Clinical Specimens in Mycobacteria Growth Indicator Tube Medium. *New Microbiol.* **2018**, *41*, 1121–7138.

(31) Bandyopadhyay, D.; Gupta, S.; Paine, S. K.; Gupta, S.; Banerjee, S.; Bhattacharya, S.; Gachhui, R.; Bhattacharya, B. Rapid Identification of Mycobacterium Species with the Aid of Multiplex Polymerase Chain Reaction (PCR) From Clinical Isolates. *Open Microbiol. J.* **2010**, *4* (1), 93–97.

(32) Banaiee, N.; Bobadilla-del-Valle, M.; Riska, P.; Bardarov, S.; Small, P.; Ponce-de-Leon, A.; Jacobs, W.; Hatfull, G. F.; Sifuentes-Osornio, J. Rapid Identification and Susceptibility Testing of Mycobacterium Tuberculosis from MGIT Cultures with Luciferase Reporter Mycobacteriophages. *J. Med. Microbiol.* **2003**, *52* (7), 557–561.

(33) Mousa, S.; Bohunicky, B. Biosensors: The New Wave in Cancer Diagnosis. *Nanotechnol. Sci. Appl.* **2010**, *4* (1).

(34) Chauhan, N.; Maekawa, T.; Kumar, D. N. S. Graphene Based Biosensors—Accelerating Medical Diagnostics to New-Dimensions. *J. Mater. Res.* **2017**, *32* (15).

(35) Soper, S. A.; Brown, K.; Ellington, A.; Frazier, B.; Garcia-Manero, G.; Gau, V.; Gutman, S. I.; Hayes, D. F.; Korte, B.; Landers, J. L.; Larson, D.; Ligler, F.; Majumdar, A.; Mascini, M.; Nolte, D.; Rosenzweig, Z.; Wang, J.; Wilson, D. Point-of-Care Biosensor Systems for Cancer Diagnostics/Prognostics. *Biosens. Bioelectron.* **2006**, *21* (10), 1932–1942.

(36) Ali, J.; Najeeb, J.; Ali, M. A.; Aslam, M. F.; Raza, A. Biosensors: Their Fundamentals, Designs, Types and Most Recent Impactful Applications: A Review. *J. Biosens. Bioelectron.* **2017**, *8* (1).

(37) Yáñez-Sedeño, P.; Agüí, L.; Villalonga, R.; Pingarrón, J. Biosensors in Forensic Analysis. A Review. *Anal. Chim. Acta.* **2014**, *823*, 1–19.

(38) Terry, L. A.; White, S. F.; Tigwell, L. J. The Application of Biosensors to Fresh Produce and the Wider Food Industry. *J. Agric. Food Chem.* **2005**, *53* (5), 1309–1316.

(39) Baruah, S.; Dutta, J. Nanotechnology Applications in Pollution Sensing and Degradation in Agriculture: A Review. *Environ. Chem. Lett.* **2009**, *7* (3), 191–204.

(40) Mehrotra, P. Biosensors and Their Applications - A Review. *J. oral Biol. craniofacial Res.* **2016**, *6* (2), 153–159. https://doi.org/10.1016/j.jobcr.2015.12.002.

(41) Kumanan, V.; Nugen, S. R.; Baeumner, A. J.; Chang, Y. F. A Biosensor Assay for the Detection of Mycobacterium Avium Subsp. Paratuberculosis in Fecal Samples. *J. Vet. Sci.* **2009**, *10* (1), 35–42. https://doi.org/10.4142/jvs.2009.10.1.35.

(42) Shojaei, T. R.; Mohd Salleh, M. A.; Tabatabaei, M.; Ekrami, A.; Motallebi, R.; Rahmani-Cherati, T.; Hajalilou, A.; Jorfi, R. Development of Sandwich-Form Biosensor to Detect Mycobacterium Tuberculosis Complex in Clinical Sputum Specimens. *Brazilian J. Infect. Dis.* **2014**, *18* (6), 600–608. https://doi.org/10.1016/j.bjid.2014.05.015.

(43) Ahmed, A.; Rushworth, J. V.; Hirst, N. A.; Millner, P. A. Biosensors for Whole-Cell Bacterial Detection. *Clin. Microbiol. Rev.* **2014**, *27* (3), 631–646. https://doi.org/10.1128/CMR.00120-13.

(44) Bryan, T.; Luo, X.; Bueno, P. R.; Davis, J. J. An Optimised Electrochemical Biosensor for the Label-Free Detection of C-Reactive Protein in Blood. *Biosens. Bioelectron.* **2013**, *39* (1), 94–98. https://doi.org/10.1016/j.bios.2012.06.051.

(45) Zhao, S.; Yang, W.; Lai, R. Y. A Folding-Based Electrochemical Aptasensor for Detection of Vascular Endothelial Growth Factor in Human Whole Blood. *Biosens. Bioelectron.* **2011**, *26* (5), 2442–2447. https://doi.org/10.1016/j.bios.2010.10.029.

(46) Bonham, A. J.; Paden, N. G.; Ricci, F.; Plaxco, K. W. Detection of IP-10 Protein Marker in Undiluted Blood Serum via an Electrochemical E-DNA Scaffold Sensor. *Analyst* **2013**, *138*, 5580–5583. https://doi.org/10.1039/c3an01079a.

(47) Vallée-Bélisle, A.; Ricci, F.; Uzawa, T.; Xia, F.; Plaxco, K. W. Bioelectrochemical Switches for the Quantitative Detection of Antibodies Directly in Whole Blood. *J. Am. Chem. Soc.* **2012**, *134* (37), 15197–15200.

(48) Ferguson BS, Hoggarth DA, Maliniak D, et al. Real-Time, Aptamer-Based Tracking of Circulating Therapeutic Agents in Living Animals. *Sci.Transl. Med.* **2013**, *5* (213).

(49) Fetter, L.; Richards, J.; Daniel, J.; Roon, L.; Rowland, T. J.; Bonham, A. J. Electrochemical Aptamer Scaffold Biosensors for Detection of Botulism and Ricin Toxins. *Chem. Commun.* **2015**, 8–11. https://doi.org/10.1039/C5CC05933J.

(50) Gooding, J. J. Electrochemical DNA Hybridization Biosensors. *Electroanalysis* **2002**, *14* (17), 1149–1156.

(51) Liu, A.; Wang, K.; Weng, S.; Lei, Y.; Lin, L.; Chen, W.; Lin, X.; Chen, Y. Development of Electrochemical DNA Biosensors. *TrAC Trends Anal. Chem.* **2012**, *37*, 101–111.

(52) Mayer, M. D.; Lai, R. Y. Effects of Redox Label Location on the Performance of an Electrochemical Aptamer-Based Tumor Necrosis Factor-Alpha Sensor. *Talanta* **2018**, *189*, 585–591.

(53) Briken, V.; Porcelli, S. A.; Besra, G. S.; Kremer, L. Mycobacterial Lipoarabinomannan and Related Lipoglycans: From Biogenesis to Modulation of the Immune Response. *Mol. Microbiol.* **2004**, *53* (2), 391–403.

(54) Tang, X.-L.; Wu, S.-M.; Xie, Y.; Song, N.; Guan, Q.; Yuan, C.; Zhou, X.; Zhang, X.-L. Generation and Application of SsDNA Aptamers against Glycolipid Antigen ManLAM of Mycobacterium Tuberculosis for TB Diagnosis. *J. Infect.* **2016**, *72* (5), 573–586.

(55) Sun, X.; Pan, Q.; Yuan, C.; Wang, Q.; Tang, X.-L.; Ding, K.; Zhou, X.; Zhang, X.-L. A Single SsDNA Aptamer Binding to Mannose-Capped Lipoarabinomannan of Bacillus Calmette–Guérin Enhances Immunoprotective Effect against Tuberculosis. *J. Am. Chem. Soc.* **2016**, *138* (36), 11680–11689. https://doi.org/10.1021/jacs.6b05357.

(56) Markham, N. R.; Zuker, M. DINAMelt Web Server for Nucleic Acid Melting Prediction. *Nucleic Acids Res.* **2005**, *33*. https://doi.org/10.1093/nar/gki591.

(57) Li, L.; Zhao, H.; Chen, Z.; Mu, X.; Guo, L. Aptamer Biosensor for Label-Free Square-Wave Voltammetry Detection of Angiogenin. *Biosens. Bioelectron.* **2011**, *30* (1), 261–266.

(58) Bonham, A. J. Peakfinder: Square-Wave Voltammetry Peak Measurement Code.

(59) Rowe, A. A.; White, R. J.; Bonham, A. J.; Plaxco, K. W. Fabrication of Electrochemical-DNA Biosensors for

the Reagentless Detection of Nucleic Acids, Proteins and Small Molecules. *J. Vis. Exp.* **2011**, No. 52, e2922. https://doi.org/10.3791/2922.

(60) Vallee-Belisle, A.; Ricci, F.; Plaxco, K. W. Thermodynamic Basis for the Optimization of Binding-Induced Biomolecular Switches and Structure-Switching Biosensors. *Proc. Natl. Acad. Sci. U. S. A.* **2009**, *106* (33), 13802–13807. https://doi.org/0904005106 [pii] 10.1073/pnas.0904005106 ET - 2009/08/12.

(61) Anderson, B. J.; Larkin, C.; Guja, K.; Schildbach, J. F. Using Fluorophore-Labeled Oligonucleotides to Measure Affinities of Protein–DNA Interactions. *Fluoresc. Spectrosc. Methods Enzymol.* **2008**, *450*, 253–272.

(62) Jing, M.; Bowser, M. T. Methods for Measuring Aptamer-Protein Equilibria: A Review. *Anal. Chim. Acta* **2011**, *686* (1–2), 9–18. https://doi.org/10.1016/j.aca.2010.10.032.

(63) Dauphin-Ducharme, P.; Plaxco, K. W. Maximizing the Signal Gain of Electrochemical-DNA Sensors. *Anal. Chem.* **2016**, *88* (23), 11654–11662. https://doi.org/10.1021/acs.analchem.6b03227.

(64) White, R. J.; Phares, N.; Lubin, A. A.; Xiao, Y.; Plaxco, K. W. Optimization of Electrochemical Aptamer-Based Sensors via Optimization of Probe Packing Density and Surface Chemistry. *Langmuir* **2008**, *24* (18), 10513–10518. https://doi.org/10.1021/la800801v.

(65) Schorey, J. S.; Sweet, L. The Mycobacterial Glycopeptidolipids: Structure, Function, and Their Role in Pathogenesis. *Glycobiology* **2008**, *18* (11), 832–841. https://doi.org/10.1093/glycob/cwn076.

(66) Bayat, P.; Nosrati, R.; Alibolandi, M.; Rafatpanah, H.; Abnous, K.; Khedri, M.; Ramezani, M. SELEX Methods on the Road to Protein Targeting with Nucleic Acid Aptamers. *Biochimie* **2018**, *154*, 132–155.